40th Fluid Dynamics Conference and Exhibit
28 June - 1 July 2010, Chicago, Illinois

AIAA 2010-4463

Experimental and Numerical Study of Flow Topology Past Micro Vortex Generators

Frank K. Lu,* Adam J. Pierce,† Yusi Shih,† Chaoqun Liu‡ and Qin Li§
University of Texas at Arlington, Arlington, Texas, 76019

Detailed experimental and numerical visualizations of the flow past a micro vortex generator (MVG) in the form of a ramp with swept sides in a Mach 2.5 flow revealed a complex near-field topology. The incoming flow separated over the leading edge of the MVG despite the ramp angle being below the threshold for incipient separation. The separation over the MVG protuberance produced a weak trailing horseshoe vortex system. The attachment line shows a saddle/foci combination on each side of a nodal point of attachment. The flow over the top of the MVG separated off the slant edges to produce a large primary vortex pair. This large primary vortex pair induced two secondary vortex filament pairs, one off the top of the MVG and another at the corner of the MVG with the flat plate. Extra complexities were revealed at the trailing edge with at least two pairs of saddle/foci combinations observed. It is postulated that vortex filaments spring from the various saddle/foci combinations as these were not observed experimentally or computationally. Symmetry breaking due to flow unsteadiness was also observed in the MVG wake.

I. Introduction

A SHOCK/BOUNDARY-LAYER interaction (SBLI) flow control technique proposed recently is to distribute an array of micro vortex generators (MVGs), whose height is less than the boundary layer thickness, ahead of the region with adverse flow conditions.[1–18] These MVGs are thought to function similarly to conventional vortex generators in energizing the boundary layer via entrainment of the freestream flow by trailing vortices. The main difference between MVGs and conventional vortex generators is that the former produces less drag. MVGs have apparently been deployed in practice and appear to be beneficial under certain circumstances, such as the low-speed performance of large transport aircraft[19] and proposed for potential application in supersonic inlets[13] and cabin noise reduction.[20] One form of MVG is a wedge-shaped ramp at a shallow angle, as depicted in Fig. 1.

Initial studies were conducted at low speeds and then extended to supersonic flows where the interest lies primarily in reducing or eliminating the separation zone of strong SBLIs. These high-speed studies generally were conducted with an impinging shock due to its relevance in inlets.

While there is evidence of the benefits of MVGs, the underlying physical mechanisms as to how they affect the boundary layer and especially separated SBLIs remains a topic of ongoing research. It appears that some of the ideas regarding the flow past an MVG are derived from observations of conventional vortex generators at low speeds. Thus, the belief is that the flow past an MVG possesses a horseshoe vortex wrapping around

*Professor and Director, Aerodynamics Research Center, Department of Mechanical and Aerospace Engineering. Associate Fellow AIAA.
†Graduate Research Assistant, Aerodynamics Research Center, Department of Mechanical and Aerospace Engineering. Student Member AIAA.
‡Professor and Director, Center for Numerical Simulation and Modeling, Mathematics Department. Associate Fellow AIAA.
§Visiting Professor, Mathematics Department. Member AIAA.

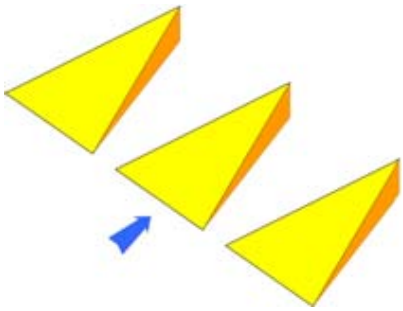

Figure 1. Schematic of an MVG array.

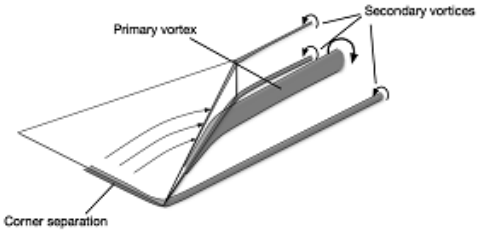

Figure 2. Existing model of multiple trailing vortices shed from an MVG.[8]

the leading edge of the MVG and trailing off the leading-edge tips. In general, horseshoe vortices are expected in boundary layer flows past a surface-mounted protuberance, even in supersonic speeds.[21] While multiple separation zones are formed if the object is bluff, the streamlined MVG protuberance is expected to produce only a single separation zone off its leading edge, as is evidently so. Also, the horseshoe vortex is expected to be weak and, in fact, it has not been properly observed experimentally or numerically except via the telltale evidence from surface flow visualization.

Figure 2 is a schematic of the existing model of the flow past an MVG. Beside the horseshoe vortex, a pair of primary and two pairs of secondary trailing vortices are thought to exist. It can be noted that Herges et al.[11] identified only a pair of secondary trailing vortices. Babinsky and co-workers,[3,5,8] from surface flow visualization, and Lee et al.,[16] from large eddy simulations, suggested that the pair of counter-rotating (primary) vortices trails downstream of an MVG. The experiments indicated a small separation zone ahead of the compression zone which creates a weak horseshoe vortex on either side of a region devoid of pigment where a herringbone pattern can be seen. This herringbone pattern, as observed in other three-dimensional flows, is considered to be the result of open separation.[22] This open separation zone consists of the large (primary) trailing vortex on each side of the MVG, counter-rotating with respect to each other, the direction of which is indicated in Fig. 2.

Babinsky et al.[8] noted that the herringbone pattern and two bright lines fade about two MVG lengths downstream. They suggested that this is due to the primary trailing vortices lifting off the surface from their mutual upwash, a notion also proposed by Herges et al.[11] Other than the primary trailing vortex pair, Babinsky and coworkers found two further pairs of trailing vortices, a pair shed from the top of the MVG and another from the junction between the slant sides of the MVG and the floor. Finally, Babinsky et al.[8] suggested that there is a small separation around the trailing edge of the ramp although this statement appears incomplete without being properly identified.

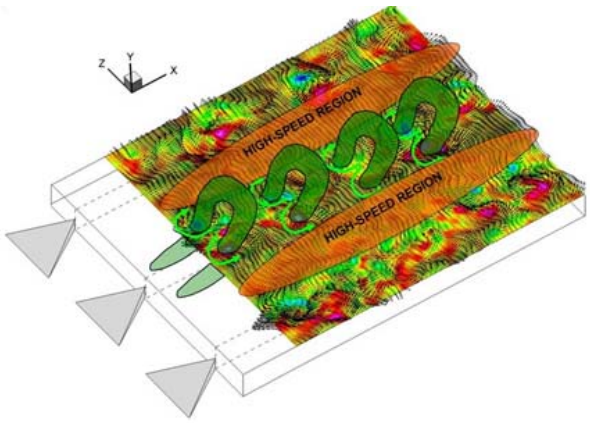

Figure 3. Conceptual schematic of flow downstream of an MVG array, showing the presence of hairpin vortices.[14]

Blinde et al.,[14] through detailed stereoscopic particle image velocimetry, proposed a model shown in Fig. 3. The schematic shows hairpin vortices streaming downstream from each MVG. A high-speed region exists between the streaming hairpin vortices. These observations appear to confirm the observation by Babinsky et al.[8] that the primary trailing

vortices lift off the surface which, as suggested by Blinde et al., leads to the formation of hairpin vortices.

Most recently, Li and Liu[17,18] using high-order, large eddy simulations, found a complex flowfield arising from the MVG. Other than the horseshoe vortex, the trailing vortices shed from the MVG suffer a Kelvin–Helmholtz-like breakdown due to an inflectional surface in the so-called velocity deficit region downstream of the MVG to form vortex rings. The vortex rings then propagate to a downstream shock/boundary-layer interaction region. This discovery of vortex rings may be considered to be a further refinement of Blinde et al.'s[14] discovery and awaits experimental confirmation.

II. Experiment

A. Facility and Test Hardware

For brevity, only a summary of the experiments is provided with details available in [23]. The experiments were performed in a blowdown wind tunnel at a Mach number of 2.47 ± 0.005. The tunnel operation was controlled by a host computer which opened the control valve to reach steady-state pressure conditions in about 2–3 s.[24] The total pressure was kept at 200 ± 6 kPa (29 ± 0.9 psia). The duration of the flow visualization experiments was less than 10 s long which resulted in a total temperature drop of only 1–2 K. Thus, despite the blowdown nature of the tunnel, the temperature can be considered to be steady for the present experiments. With the relatively steady total pressure and temperature, the unit Reynolds number can also be considered to be steady at 43 million per m.

The test section was 15.2 cm square × 81.28 cm long (6 in.^{2} × 2.67 ft). It was outfitted with extensive optical access from both sides and from the top. A flat plate, 73 cm (28.75 in.) long, with a sharp leading edge of 15 deg, was mounted in the test section[25] over which a boundary layer was developed naturally as shown schematically in Fig. 4. The flat plate was made in layers supported by a sharp-tipped rail on each side. The top layer which formed the test surface was made of a number of small, thin plates. These plates butt tightly against each other to form a continuous, flat surface. This modular design allowed for quick configuration changes. A cavity below the top surface allowed pressure tubing, transducer wiring and other elements to be placed. The wiring and tubing were channeled to the rear, either from the side of the test section or from the side of the diffuser, to outside the wind tunnel. A bottom cover encases the cavity.

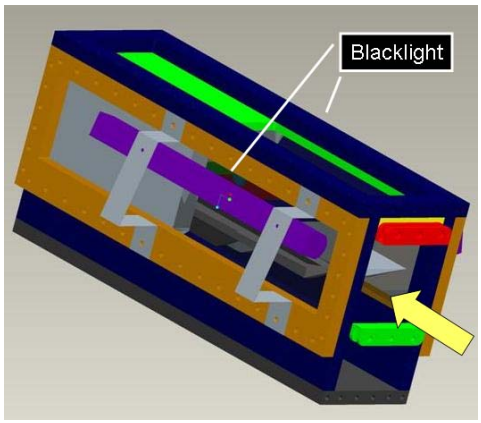

Figure 4. Test section schematic. Flow from right to left.

An MVG array was mounted with the leading edge located 272 mm (10.7 in.) downstream of the leading edge of the flat plate. Figure 5 shows the array of five MVGs. Each MVG was 12.95 mm (0.51 in.) long and 1.57 mm (0.062 in.) high. The front of the MVG was 11.7 mm (0.46 in.) wide. The center-to-center spacing between the MVGs was 30.5 mm (1.2 in.). Two styles of MVGs were fabricated based on the designs from [18], with the trailing edge angle of either 45 or 70 deg, these being subsequently called MVG45 and MVG70 respectively.

B. Diagnostics

The diagnostics consisted of surface flow visualization, described in detail in [26], in which bands of fluorescent mixture were painted along the surface of the plate ahead of the area of interest. A mixture of kerosene and fluorescent chalk with a small quantity of silicone oil was found to be suitable. Two recording techniques were used: a high-definition camcorder (Canon Vixia HF S10) and a high-resolution DSLR (Nikon D300S). As shown in Fig. 4, "blacklight" tubes (Utilitech Model Gu9721P-T8-BKI) were placed on either side of

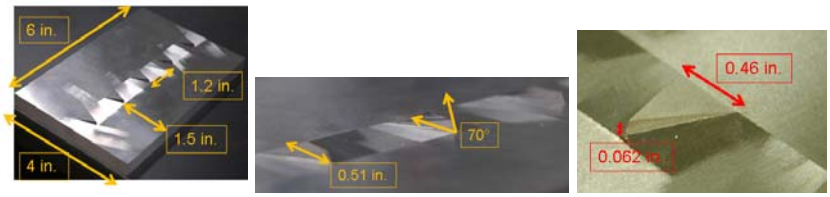

Figure 5. Micro-vortex generator array.

the test section to illuminate the mixture without turning off the ambient fluorescent lighting. The digital images (still or video) were processed as necessary to reveal small or obscure features.

III. Computations

A high-order large eddy simulation was previously reported and is only briefly outlined here.[17,18] The conservation equations were solved in nondimensional form with a fifth-order WENO scheme for the convective terms. Adiabatic, zero normal pressure gradient and no slip conditions were applied on the wall.

A. Governing Equations and Discretization

The governing equations are the non-dimensional Navier-Stokes equations in conservative form written in Cartesian coordinates. A fifth-order WENO scheme was used to discretize the convective terms.[27] A fourth-order central difference scheme was used to discretize the second-order transport terms. Temporal discretization was an explicit, third-order TVD-type Runge-Kutta scheme.[28]

1. Boundary Conditions

Adiabatic, zero normal pressure gradient and non-slip conditions were used on solid surfaces. Only the leading shock from the MVG will reach the upper boundary. This shock is weakened by the expansion waves from the trailing edge of the MVG so that no visible reflections are observed. Even if there were reflections, these will exit the domain without impinging on the boundary layer. The outflow boundary conditions were specified as a type of characteristic-based condition which can handle the outgoing flow without reflection.[18] The inflow conditions were generated by first inputting a turbulent mean profile for the streamwise velocity, scaled to the local displacement thickness and the freestream velocity. The pressure in the inflow plane was constant and was the freestream value. The temperature profile was obtained using the Walz equation relating velocity and temperature for an adiabatic wall, with a recovery factor of 0.85.[29] Random fluctuations were added on the primitive variables, that is, u, v, w, p, ρ. Such inflow conditions are, of course, not the exact solutions of the Navier–Stokes equations. However, the flow solver will adjust and modulate the flow into a weakly turbulent one as it propagates downstream.

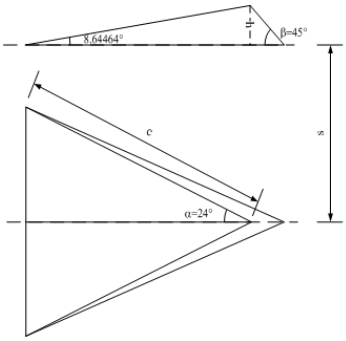

Figure 6. MVG geometry for LES.

2. Code Validation

The code was validated against an asymptotic solution to the Mach 4 flow past a semicircular body. Pressure distributions were oscillation free and the convergence was achieved with a six orders in the decrease of the

residuals. The code was also validated by yawing the semicircular body to produce a three-dimensional flow.

3. Grid Generation

Body-fitted grids were used to preserve the geometry and to reduce numerical errors in using the fifth-order WENO scheme. The MVG geometry with a trailing edge inclined at 45 deg is shown in Fig. 6. Another MVG configuration, with the same height, had the trailing edge inclined at 70 deg. A total of $n_{span} \times n_{normal} \times n_{stream} = 128 \times 192 \times 1\,600 = 32\,321\,000$ grids were used. Details of grid generation can be found in [18].

IV. Results and Discussion

A. Surface Flow at the MVG Leading Edge

To fully appreciate the complex flow topology arising from such an apparently simple geometry requires complementary high resolution experiments and computations. Figure 7 shows the surface oil flow pattern from the experiment and the top view of the surface streamlines from the computations. In the terminology of three-dimensional flows[22,30–32] there is a closed separation at the leading edge of the MVG. The separation bubble is smaller in the experimental result than in the computational one which can be attributed to the lower Reynolds number of the latter. Note that the presence of separation, also observed by Babinsky et al.[8] at Mach 2.5, is below the incipient threshold of about 16 deg as reported in a number of data compilations.[33–35] (See also Herges et al.[11] whose results showed a similar feature at Mach 1.4.) The leading-edge separation was apparently not resolved in earlier numerical simulations[6] nor reported in various experimental and numerical investigations. An obvious reason for separation induced by the small leading edge angle is that the effective Mach number is lower due to the MVG being submerged in the boundary layer. The extent of the separation in the numerical result is larger than that of the experiment. This can be attributed to the lower Reynolds number of the former. Unlike protuberances whose heights extend outside of the boundary layer, classified as producing a noninfinite SBLI,[36] which produces multiple separation zones, the interaction induced by an MVG is weak indeed.

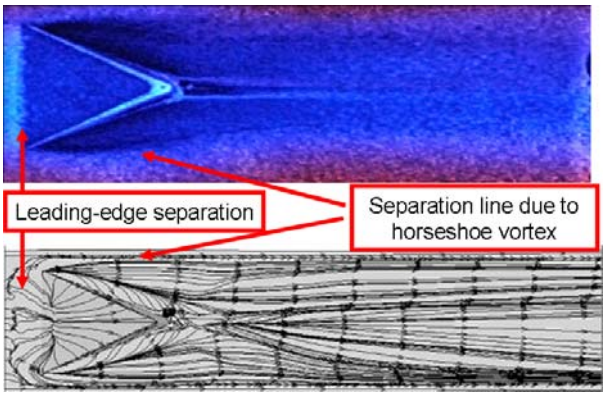

Figure 7. Surface flow visualization for MVG45 (top view).

The three-dimensional attachment line must curve and intersect the leading-edge tips to ensure that the velocity gradient remains finite. The reattachment line then continues downstream on the flat plate. Topologically, a focus and saddle pair must occur. These features are visible in Fig. 8 which shows a node of attachment at the centerline. A pair of focal nodes and saddles can be seen on the attachment line emanating on either side of this node. Tobak and Peake[30] calls the dividing surface from the focus a "horn-type." These features are not visible in any flow visualizations thus far.

B. Surface Flow at the MVG Side

Some other details can be seen in the combined visualizations from different viewing angles, see Figs. 8 and 9. Numerical simulations of the surface streamlines over the MVG show that they spill over the slant edges. (For an analogous flow of separation from a chevron-shaped backward-facing step, see [37]. The slant edge is literally a separation line in what Tobak and Peake,[30] following Wang,[22] calls a local separation line. (The

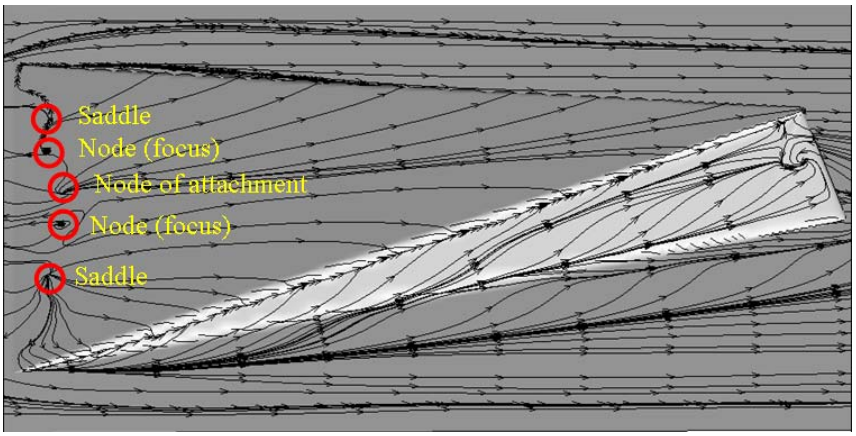

Figure 8. Close-up side view of MVG surface topology.

local separation line does not originate from a saddle point, unlike the global separation that produced the horseshoe vortex.) The flow detaching from the slant edges attaches on the flat plate and spirals downstream as evidenced by the herringbone pattern. Such a flow structure is required to satisfy the boundary conditions on the flat plate and the dynamic pressure constraint imposed by the mainstream on the side and top of the MVG.

In contrast, the figure of the experimental result does not show the herringbone feature clearly; this is also not clearly visible in [8, 11]. The surface flow spillage past the slant edges is clearly seen, however, in video recordings.[26] Further, instead of a herringbone pattern, the experimental visualization shows a dark region hugging the corner of the MVG and the flat plate. This indicates that the pigment in this region is scoured away by high shear forces that reinforces the notion of an open, three-dimensional separation from the numerical simulations.[30–32] This is unlike the closed separation at the leading edge of the MVG. Moreover, the slant edges in the experimental visualization are outlined by a bright fringe which, obviously, cannot be seen in the numerical simulation. The bright line, upon further investigation, is found to be due to an accumulation of the pigment that is indicative of attachment.[38] This is elaborated next.

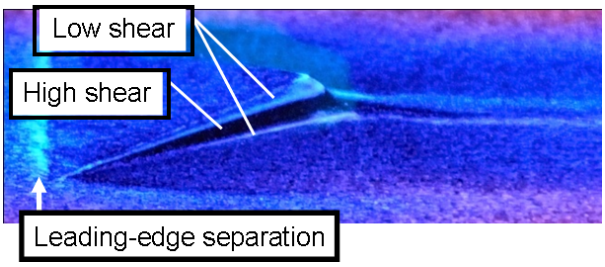

Figure 9. Surface flow visualization (side view).

To further investigate the bright lines at the slant edges seen in Fig. 7, the side view of the experimental visualization in Fig. 9 shows that there are in fact two bright bands, one off the top of the MVG and the other at the junction between the MVG and the flat plate. Using these features as guidance for interpreting the numerical simulations, it can be seen that the latter also reveals the same extremely thin separation and attachment zones off the MVG top and at the MVG junction with the flat surface. The numerical visualization, moreover, shows that the herringbone pattern extends up the side of the MVG, a telltale sign of the large vortex spiraling downstream associated with open separation. Further, the regularity of the herringbone pattern breaks down toward the rear of the MVG. This breakdown reveals further complexities in the surface flow in that region.

C. Surface Flow at the MVG Rear

The surface flow at the rear of the MVG is now examined in detail. The view from the back looking upstream is shown in Fig. 10. The experimental visualization shows a bright smear on either side of the trailing edge. More details are revealed in the numerical visualization which shows that the surface streamlines converge on a pair of spiral foci, one on each side as previously reported in [17, 18]. These point singularities, known as foci, require that the surface streamlines lift off the surface,[30–32] which have consequences in interpreting the downstream flow.

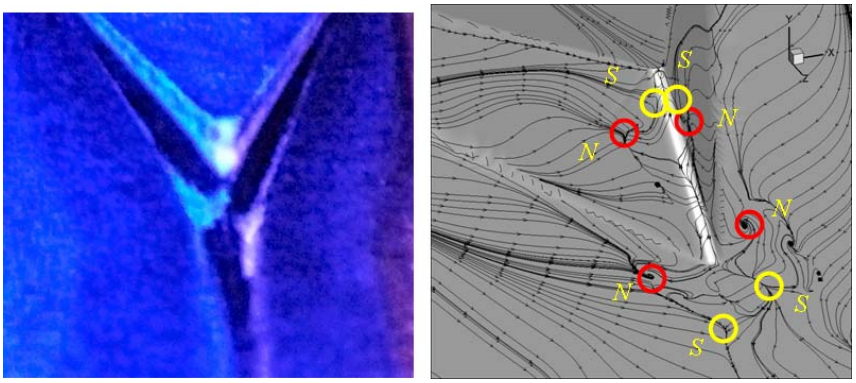

Figure 10. Surface flow visualization (rear looking forward): S = saddle, N = node (focus).

These small but significant features are difficult to visualize experimentally due to added complications in that the flow in this region is unsteady. The unsteadiness can be deduced from the experimental visualization presented in Fig. 10 as a smearing of the two bright features and is even more obvious in video recordings. Through nonlinear filtering,[26] the original experimental surface visualization was enhanced and one of the images is shown in Fig. 11, side-by-side with the numerical visualization. The enhanced experimental image shows the two foci clearly as an accumulation of pigment.

Tobak and Peake[30] state that "the focus invariably appears on the surface in company with a saddle point." To further quote Tobak and Peake:

> *"Together they* [that is, the focus and saddle point combination] *allow a particular form of global flow separation. One leg of the (global) line of separation emanating from the saddle point winds into the focus to form the continuous curve on the surface from which the dividing surface stems. The focus on the wall extends into the fluid as a concentrated vortex filament, while the dividing surface rolls up with the same sense of rotation as the vortex filament."*

The numerical visualization affirms the above statements by revealing a saddle in coexistence with a focus. One can also deduce that a vortex filament emanates from a focus with a dividing (separation) surface wrapped around it. Returning to Fig. 10, the numerical visualization reveals a total of two spiral foci near the rear of each side of the MVG[39] although no attempt was made to capture this spiral experimentally.

In addition, the experimental visualization in Fig. 7 shows a pair of bright lines trailing and eventually disappearing downstream at about two MVG ramp lengths. This is also observed by Babinsky et al.[8] and Herges et al.[11] both of whom suggested that the disappearance is associated with the primary vortices lifting off the surface as a result of mutual upwash between these vortices. However, this premise may be incomplete as such a liftoff has to be rapid for the sudden disappearance. In other studies on the wakes of protuberances,[21] the trailing vortices were found leave a signature for a long distance downstream that is inconsistent with the vortices lifting off the surface. Thus, the proposed mechanism for such a rapid liftoff due to the mutual interaction of the two trailing primary vortices may be insufficient. Further, with the evidence from Blinde et al.[14] of a train of hairpin vortices, it appears that a possible mechanism may be the breakdown

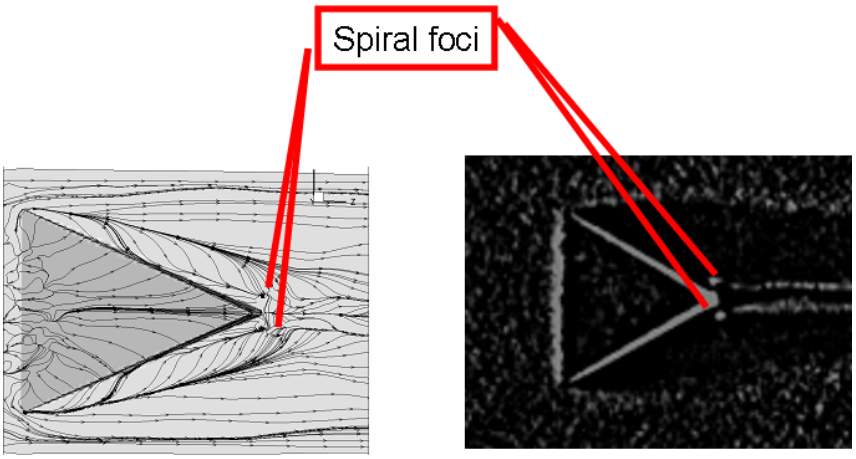

Figure 11. Identifying the spiral foci at the rear of an MVG.

of the primary trailing vortex pair. The numerical visualization does not show a disappearance of the two bright lines but only shows a necking down of the separation lines followed by a subsequent divergence. More discussion of this can be found in [40] as the present paper focuses on the complex nearfield topology.

D. Off-Surface Topological Features

Surface flow visualization, supplemented by lightsheet visualization, surface pressure measurements and Pitot surveys, has been successful in constructing complex, three-dimensional flowfields. Examples of success includes the flow over the leeside of delta wings,[41] supersonic corner flows[42] and three-dimensional shock/boundary layer interactions.[36] While purely experimental approaches have met with success, there is also presentation of joint experimental and numerical studies for educing flow physics. One area where such a joint study can benefit due to complementary capabilities is in visualization.

In the present study, numerical visualizations of some near-surface streamlines are shown in Fig. 12. The figure clearly shows that the incoming, parallel streamlines are deflected downward and outward past the slant edge of the MVG. The streamlines then rotate downward and are deflected inward to satisfy the solid boundary condition of the flat surface and the high dynamic pressure above. This flow pattern is consistent with the herringbone pattern seen in the numerical surface streamlines and in the experimental surface flow visualizations (Fig. 7).

A common method for visualizing vortex structures in numerical simulations is to plot iso-surfaces of λ_2, which is the second eigenvalue of the 3×3 matrix comprised of the velocity gradient,[43] that is,

$$M_{ij} = \sum_{k=1}^{3} (\Omega_{ik}\Omega_{kj} + S_{ik}S_{kj}) \tag{1}$$

where

$$\Omega_{ij} = \frac{1}{2}\left(\frac{\partial u_i}{\partial x_j} + \frac{\partial u_j}{\partial x_i}\right) \text{ and } S_{ij} = \frac{1}{2}\left(\frac{\partial u_i}{\partial x_j} - \frac{\partial u_j}{\partial x_i}\right) \tag{2}$$

Figure 13 shows iso-surfaces of λ_2 using a small negative value for visualization. This figure shows thin strips at the top and bottom edges of the MVG to be vortices. An additional vortex tube emanates from the spiral point, partly obscured by the vortex streaming from the lower edge of the MVG. At the present moment, the vortex filaments from the MVG side or associated with the leading-edge attachment are not visualized.

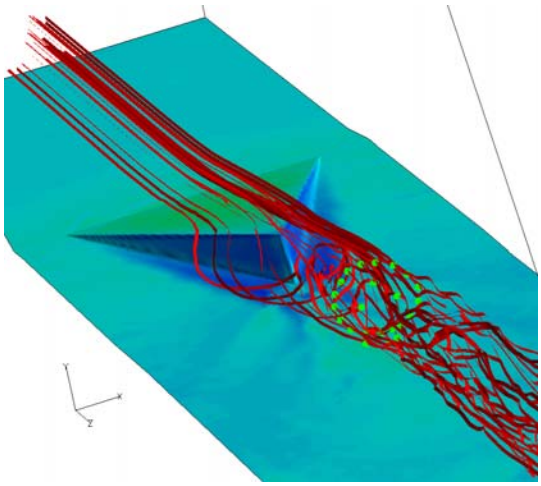

Figure 12. Near-surface streamlines obtained numerically.[17, 18]

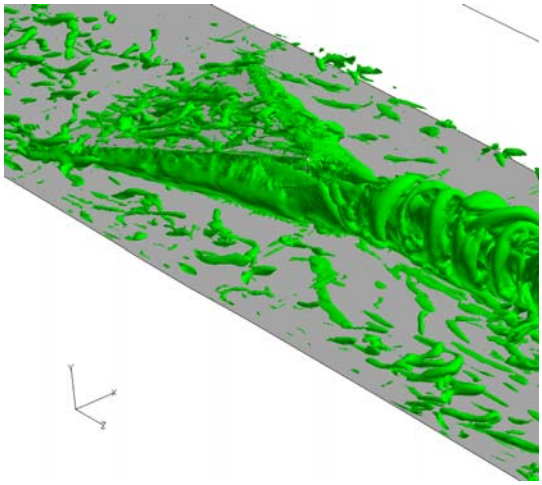

Figure 13. Iso-surfaces of λ_2.[17, 18]

E. Topological Model

The topology around the MVG which is consistent with topological rules[30] can now be completed. It should be noted that these rules usually cannot predict the types of singularities that can occur in a flowfield but that they can be very effective in interpreting topological features. Figure 14 shows the incoming surface streamlines stagnating ahead of the MVG giving rise to a saddle point of separation N_S, bifurcating into a global separation line S_H where the subscript H denotes "horseshoe." Topologically, there must be either a saddle or a nodal point of attachment. The presence of the horseshoe vortex requires the choice of a nodal point of attachment where the surface streamlines converge toward it (see Fig. 5(a) of [30]). The nodal point of attachment is shown in Fig. 14 as N_A which is the convergence of the reattachment line A_H. This terminology also makes it clear that N_S is a saddle point—if it was a node, the surface streamlines must converge to it as is evidently not the case.

The surface streamlines in the separation zone point upstream toward S_H. To ensure that velocity gradients remain finite, the surface streamlines leave the top of the MVG such that the attachment line must curve to terminate at the leading-edge tips. The attachment line then continues on the flat surface. The separation zone between S_H and A_H that develops along the sides of the obstacle is commonly called a horseshoe vortex. However, the vortex filament V_F that emanates from the node/saddle combination on either side of the attachment node has not been visualized and is thus indicated in Fig. 14.

The primary vortex V_P is formed by flow leaving the top of the MVG. In other words, the swept trailing edges of the MVG form a separation line. The attachment line of the primary vortex is due to an impinging jet flow constrained by the high dynamic pressure on the MVG side and top to swirl inward. This inward swirling flow gives rise to the herringbone pattern in surface visualizations. The confluence of the primary vortex and the two secondary vortices yields a complicated topology toward the trailing edge of the MVG that is clearly evident in the numerical visualization of Figs. 10 and 11.

In general, the number of secondary vortices that can emanate from tip of the MVG is unspecified and depends on the geometry. The degenerate case of no separation can happen in the limiting situation of an infinitely small MVG where one can imagine that the flow remains attached. The case with one open separation, that is, one secondary vortex, is possible for a smoothly shaped MVG bump, where the flow again spills off the top but now encounters a sharp change in topography between the MVG and the flat plate. In the present case where the MVG has flat sides, the flow spills off the top but the finite velocity gradient now requires an open separation on top and another at the corner of the MVG and flat plate. One can

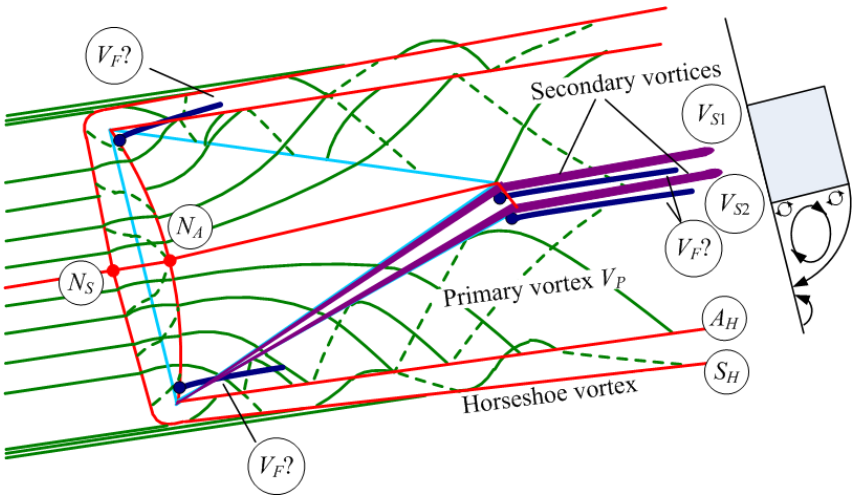

(a)

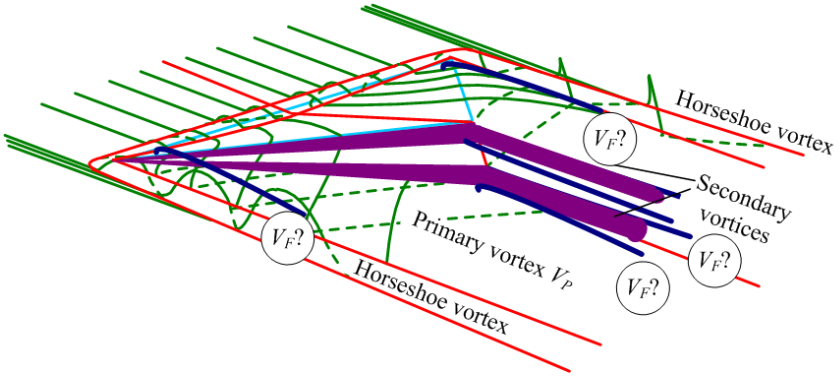

(b)

Figure 14. The postulated mean flowfield topology past an MVG (dashed lines indicate surface flow).

imagine more complicated possibilities for MVG configurations with higher-order polygonal cross-sections. The vortices identified here are known as the primary vortex V_P due to the flow spillage of the MVG top and the two secondary vortices V_{S1} and V_{S2} to satisfy the finite velocity gradient conditions. These are shown in Fig. 14 together with their associated separation and attachment lines. Other topological features at the rear of the MVG will be described next.

As stated above, the occurrence of a spiral is invariably associated with a saddle point. A close examination of the numerical visualization in Fig. 10 shows that the surface streamlines on the trailing edge and near the top are directed downward from the top and upward from the bottom. This is counter to the surface flow pattern due to the vortex filament at the top of the MVG slide. Therefore, a *particular line* must exist between these two regions that act as barriers. Tobak and Peake[30] citing Lighthill,[44] showed adjacent nodal points associated with a particular line. In Lighthill's example, these are attachment nodes whereas in the present example, the nodes are separation ones.

Returning to Fig. 14, the complete topology of the flow past an MVG in supersonic flow can now be presented together with the associated singularities. These are:

- A weak horseshoe vortex that wrap around the MVG due to leading-edge separation; one saddle point of separation + one nodal point of attachment + a pair of saddle/node (spiral) (dividing surface or vortex filament postulated but not seen), a global separation and global reattachment line
- A pair of large primary vortices shed off the sides of the MVG; a local separation and local reattachment line
- Two pairs of secondary vortices on each side of the MVG, emanating from the MVG tip, to satisfy dynamic boundary conditions
- One pair of saddle/node at the leading edge attachment line, shown as filled circles in Fig. 14
- At least one pair of saddle/node (spiral) on the flat plate and another pair of saddle/node (spiral) on the MVG side with limited evidence of vortex filaments. These saddle/node pairs are shown as filled circles in Fig. 14.

F. Symmetry Breaking

The convergence of the primary and secondary trailing vortices from both sides of the MVG does not result in a single singularity at the rear of the trailing edge that is a theoretical possibility. Instead, two singular focal points are clearly visible and they are unsteady, as evident from experimental observations. The unsteadiness arise from symmetry breaking conditions.[45–48] As pointed out by Bridges,[48] amplification of tip disturbances can create an asymmetric wake. In the present flow, disturbances arise from the turbulent field and, therefore, the likelihood of asymmetry from this cause.

V. Conclusions

A detailed experimental and computational study of the topology of a wedge-shaped, tetrahedron micro vortex generator with a flat leading edge was performed using innovative surface flow visualization techniques and high-order large eddy simulation. The micro vortex generator was placed on a flat plate over which was developed a turbulent boundary layer at Mach 2.5. The study showed the presence of a leading-edge separation below the incipient separation threshold. The leading-edge separation is channeled around the tips of the micro vortex generator to form a weak horseshoe vortex. In addition, the geometry of the micro vortex generator spawned a complex topology consisting of a primary vortex pair and a number actual and postulated vortex filaments. The unsteadiness of the flow caused symmetry breaking to occur at the trailing edge of the micro vortex generator.

Acknowledgments

The authors gratefully acknowledge funding for this work via AFOSR Grant No. FA9550-08-1-0201 monitored by Dr. John Schmisseur. The authors thank the assistance of Rod Duke, Yusi Shih and David Whaley with the experiments. David Whaley was supported by a High School Research Internship under a Texas Youth in Technology grant from the Texas Workforce Commission, administered by Dr. J. Carter M. Tiernan.

References

[1]Anderson, B. H., Tinapple, J., and Sorber, L., "Optimal Control of Shock Wave Turbulent Boundary Layer Interactions Using Micro-Array Actuation," AIAA Paper 2006–3197, 2006.

[2]Babinsky, H., Makinson, N. J., and Morgan, C. E., "Micro-Vortex Generator Flow Control for Supersonic Engine Inlets," AIAA Paper 2007–2007, 2007.

[3]Holden, H. and Babinsky, H., "Effect of Microvortex Generators on Separate Normal Shock/Boundary Layer Interactions," *Journal of Aircraft*, Vol. 44, No. 1, 2007, pp. 89–96.

[4]Shinn, A. F., Vanka, S. P., Mani, M., Dorgan, A., and Michal, T., "Application of BCFD Unstructured Grid Solver to Simulation of Micro-Ramp Control of Shock/Boundary Layer Interactions," AIAA Paper 2007–3914, 2007.

[5]Babinsky, H. and Ogawa, H., "SBLI Control for Wings and Inlets," *Shock Waves*, Vol. 18, No. 2, 2008, pp. 89–96.

[6]Ghosh, S., Choi, J.-I., and Edwards, J. R., "RANS and Hybrid LES/RANS Simulation of the Effects of Micro Vortex Generators Using Immersed Boundary Methods," AIAA Paper 2008–3728, 2008.

[7]Anderson, B. H., Mace, J. L., and Mani, M., "Active 'Fail Safe' Micro-Array Flow Control For Advanced Embedded Propulsion Systems," AIAA Paper 2009–0920, 2009.

[8]Babinsky, H., Li, Y., and Pitt Ford, C. W., "Microramp Control of Supersonic Oblique Shock-Wave/Boundary-Layer Interactions," *AIAA Journal*, Vol. 47, No. 3, 2009, pp. 668–675.

[9]Domel, N. D., Baruzzini, D., and Miller, D. N., "CFD Results for Shock-Boundary Layer Flow Control with Micro-Ramps at Various Grid Densities," AIAA Paper 2009–4016, 2009.

[10]Galbraith, M. C., Orkwis, P. D., and Benek, J. A., "Multi-Row Micro-Ramp Actuators for Shock Wave Boundary-Layer In-teraction Control," AIAA Paper 2009–0321, 2009.

[11]Anderson, T., Kroeker, E., Elliott, G., and Dutton, J., "Micro-Ramp Flow Control of Normal Shock/Boundary Layer Interactions," AIAA Paper 2009–0920, 2009.

[12]Lee, S., Loth, E., Georgiadis, N. J., and DeBonis, J. R., "Effect of Mach Number on Flow Past Micro-Ramps," AIAA Paper 2009–4181, 2009.

[13]Rybalko, M., Loth, E., Chima, R. V., Hirt, S. M., and DeBonis, J. R., "Micro-Ramps for External Compression Low-Boom Inlets," AIAA Paper 2009–4206, 2009.

[14]Blinde, P. L., Humble, R. A., van Oudheusden, B. W., and Scarano, F., "Effects of Micro-Ramps on a Shock Wave/Turbulent Boundary Layer Interaction," *Shock Waves*, Vol. 19, No. 6, 2009, pp. 507–520.

[15]Bur, R., Coponet, D., and Carpels, Y., "Separation Control by Vortex Generator Devices in a Transonic Channel Flow," *Shock Waves*, Vol. 19, No. 6, 2009, pp. 521–530.

[16]Lee, S., Goettke, M. K., Loth, E., Tinapple, J., and Benek, J., "Microramps Upstream of an Oblique-Shock/Boundary-Layer Interaction," *AIAA Journal*, Vol. 48, No. 1, 2010, pp. 104–118.

[17]Li, Q. and Liu, C., "LES for Supersonic Ramp Control Flow Using MVG at $M = 2.5$ and $Re_\theta = 1440$," AIAA Paper 2010–0592, 2010.

[18]Li, Q. and Liu, C., "Numerical Investigation on the Effects of the Declining Angle of the Trailing Edge of MVG," AIAA Paper 2010–0714, 2010.

[19]Bohannon, K. S., "Passive Flow Control on Civil Aircraft Flaps Using Sub-Boundary Layer Vortex Generators in the AWIATOR Programme," AIAA Paper 2006–2858, 2006.

[20]Holmes, A. E., Hickey, P. K., Murphy, W. R., and Hilton, D. A., "The Application of Sub-Boundary Layer Vortex Generators to Reduce Canopy 'Mach Rumble' Interior Noise on the Gulfstream III," AIAA Paper 1987–0084, 1987.

[21]Sedney, R., "A Survey of the Effects of Small Protuberances on Boundary-Layer Flows," *AIAA Journal*, Vol. 11, No. 6, 1973, pp. 782–792.

[22]Wang, K. C., "Boundary Layer Over a Blunt Body at High Incidence with an Open-Type of Separation," *Proceedings of the Royal Society of London A*, Vol. 340, No. 1620, 1974, pp. 33–55.

[23]Pierce, A. J., *Experimental Study of Micro-Vortex Generators at Mach 2.5*, MSAE thesis, University of Texas at Arlington, 2010.

[24]Braun, E. M., Lu, F. K., Mitchell, R. R., Wilson, D. R., and Dutton, J. C., "Supersonic Blowdown Wind Tunnel Control Using LabVIEW," AIAA Paper 2008–0852, 2008.

[25]Mitchell, R. R. and Lu, F. K., "Development of a Supersonic Aerodynamic Test Section using Computational Modeling," AIAA Paper 2009–3573, 2009.

[26]Pierce, A. J., Lu, F. K., Bryant, D. S., and Shih, Y., "New Developments in Surface Oil Flow Visualization," AIAA Paper 2010–4353, 2010.

[27]Jiang, G.-S. and Shu, C.-W., "Efficient Implementation of Weighted ENO Schemes," *Journal of Computational Physics*, Vol. 126, No. 1, 1996, pp. 202–228.

[28]Cockburn, B. and Shu, C.-W., "TVB Runge–Kutta Local Projection Discontinuous Galerkin Finite Element Method for Conservation Laws II: General Framework," *Mathematics of Computation*, Vol. 52, No. 186, 1989, pp. 411–443.

[29]Walz, A., "Compressible Turbulent Boundary Layers," *The Mechanics of Turbulence: Proceedings of Colloque Internationale sur La Mechanique de la Turbulence, Marseille, August 28 to September 2, 1961*, Science Publishers, Inc., New York, 1964.

[30]Tobak, M. and Peake, D. J., "Topology of Three-Dimensional Separated Flows," *Annual Review of Fluid Mechanics*, Vol. 14, 1982, pp. 61–85.

[31]Perry, A. E. and Chong, M. S., "A Description of Eddying Motions and Flow Patterns Using Critical-Point Concepts," *Annual Review of Fluid Mechanics*, Vol. 19, 1987, pp. 125–155.

[32]Chapman, G. T. and Yates, L. A., "Topology of Flow Separation on Three-Dimensional Bodies," *Applied Mechanics Review*, Vol. 44, No. 7, 1991, pp. 329–345.

[33]Coleman, G. T. and Stollery, J. L., "Heat Transfer from Hypersonic Turbulent Flow at a Wedge Compression Corner," *Journal of Fluid Mechanics*, Vol. 56, No. 4, 1972, pp. 741–752.

[34]Elfstrom, G. M., "Turbulent Hypersonic Flow at a Wedge-Compression Corner," *Journal of Fluid Mechanics*, Vol. 53, No. 1, 1972, pp. 113–127.

[35]Spaid, F. W. and Frishett, J. C., "Incipient Separation of a Supersonic, Turbulent Boundary Layer, Including Effects of Heat Transfer," *AIAA Journal*, Vol. 10, No. 2, 1972, pp. 915–922.

[36]Settles, G. S. and Dolling, D. S., "Swept Shock Wave-Boundary Layer Interactions," *Tactical Missile Aerodynamics*, edited by M. J. Hemsch and J. N. Nielsen, Progress in Astronautics and Aeronautics, AIAA, 1986, pp. 297–379.

[37]Cao, C. and Hancock, P. E., "Boundary Layer Development After a Region of Three-Dimensional Separated Flow," *European Journal of Mechanics B/Fluids*, Vol. 23, No. 3, 2004, pp. 519–533.

[38]Squire, L. C., "The Motion of a Thin Oil Sheet Under the Steady Boundary Layer on a Body," *Journal of Fluid Mechanics*, Vol. 11, No. 2, 1961, pp. 161–179.

[39]Li, Q., Yan, Y., Liu, C., Lu, F. K., and Pierce, A. J., "Numerical and Experimental Studies on the Separation Topology of the MVG Controlled Flow at $M = 2.5$ and $Re_\theta = 1440$," to be published, 2011.

[40]Lu, F. K., Liu, C., Li, Q., Pierce, A. J., and Shih, Y., "Numerical and Experimental Study of Multi-Vortex Ring Mechanism from Micro Vortex Generators in Supersonic Flow," AIAA Paper 2008–4623, 2010.

[41]Brodetsky, M. D., Kharitonov, A. M., Krause, E., Pavlov, A. A., Nikiforov, S. B., and Shevchenko, A. M., "Supersonic Leeside Flow Topology on Delta Wings Revisited," *Experiments in Fluids*, Vol. 29, No. 6, 2000, pp. 592–604.

[42]West, J. E. and Korkegi, R. H., "Supersonic Interaction in Corner of Intersecting Wedges at High Reynolds Numbers," *AIAA Journal*, Vol. 10, No. 5, 1986, pp. 652–1323.

[43]Jiang, M., Machiraju, R., and Thompson, D. S., "Detection and Visualization of Vortices," *Visualization Handbook*, edited by C. R. Johnson and C. D. Hansen, Elsevier, 2005, pp. 295–309.

[44]Lighthill, M. J., "Attachment and Separation in Three-Dimensional Flows," .

[45]Mason, P. J. and Morton, B. R., "Trailing Vortices in the Wakes of Surface-Mounted Obstacles," *Journal of Fluid Mechanics*, Vol. 175, 1987, pp. 247–293.

[46]Crawford, J. D. and Knobloch, E., "Symmetry and Symmetry-Breaking Bifurcations in Fluid Dynamics," *Annual Review of Fluid Mechanics*, Vol. 23, 1991, pp. 341–387.

[47]Sau, A., Hwang, R. R., Sheu, T. W., and Wang, W. C., "Interaction of Trailing Vortices in the Wake of a Wall-Mounted Rectangular Cylinder," *Physical Review E*, Vol. 68, No. 5, 2003, Article No. 056303.

[48]Bridges, D. H., "Toward a Theoretical Description of Vortex Wake Asymmetry," *Progress in Aerospace Sciences*, Vol. 46, No. 2–3, 2010, pp. 62–80.